

Article

# Voltammetric Sensor Based on SeO<sub>2</sub> Nanoparticles and Surfactants for Indigo Carmine Determination

Liya Kavieva and Guzel Ziyatdinova \* 

Analytical Chemistry Department, Kazan Federal University, Kremleyevskaya 18, 420008 Kazan, Russia; liyakavieva@mail.ru

\* Correspondence: ziyatdinovag@mail.ru

**Abstract:** Indigo carmine is a widely used colorant in the food and pharmaceutical industry a high concentration of which can lead to a wide range of negative effects on human health. Therefore, colorant contents have to be strictly controlled. SeO<sub>2</sub>-nanoparticle-modified glassy carbon electrodes (GCE) have been developed as a voltammetric sensor for indigo carmine. Various types and concentrations of surfactants have been used as reagents for the stabilization of SeO<sub>2</sub> nanoparticle dispersions and as electrode surface co-modifiers. An amount of 1.0 mM cationic cetylpyridinium bromide (CPB) provides the best response of the indigo carmine on the modified electrode. The electrodes were characterized by cyclic voltammetry, chronoamperometry, and electrochemical impedance spectroscopy (EIS). SeO<sub>2</sub> nanoparticle-CPB-modified electrodes show 4.2-fold higher electroactive area vs. GCE as well as a dramatic 5043-fold decrease in the electron transfer resistance indicating effectivity of the modifier developed. The surface-controlled electrooxidation of indigo carmine proceeds irreversibly ( $\alpha_a = 0.46$ ) with the participation of two electrons and two protons. A linear dynamic range of 0.025–1.0 and 1.0–10  $\mu\text{M}$  of indigo carmine were obtained with the detection and quantification limits of 4.3 and 14.3 nM, respectively. The practical applicability of the sensor was successfully shown on the pharmaceutical dosage forms.

**Keywords:** nanoparticles; surfactants; electrochemical sensors; voltammetry; colorants; indigo carmine; pharmaceutical analysis



**Citation:** Kavieva, L.; Ziyatdinova, G. Voltammetric Sensor Based on SeO<sub>2</sub> Nanoparticles and Surfactants for Indigo Carmine Determination. *Sensors* **2022**, *22*, 3224. <https://doi.org/10.3390/s22093224>

Academic Editor: Cristina Ariño

Received: 14 March 2022

Accepted: 20 April 2022

Published: 22 April 2022

**Publisher's Note:** MDPI stays neutral with regard to jurisdictional claims in published maps and institutional affiliations.



**Copyright:** © 2022 by the authors. Licensee MDPI, Basel, Switzerland. This article is an open access article distributed under the terms and conditions of the Creative Commons Attribution (CC BY) license (<https://creativecommons.org/licenses/by/4.0/>).

## 1. Introduction

The rapid development in nanomaterials opens great opportunities for chemical sensor fabrication, in particular electrochemical ones. Non-metal oxide nanoparticles are of interest among different types of nanomaterials. Nevertheless, the attention is mainly paid to silica nanoparticles (both solid and mesoporous) to which the diverse applications such as sorbents [1,2], semiconductors [3], catalysts [4], and sensitive layers in electrochemical sensors [5–10] are reported. Further development in this field is the application of SeO<sub>2</sub> nanoparticles as an electrode surface modifier due to their excellent stability, high charge transfer, and superior electrochemical specific capacitance [11]. The electrocatalytic effect of SeO<sub>2</sub> nanoparticles has been shown on the example of a long stable water splitting process [11]. Two electrochemical sensors based on the SeO<sub>2</sub> nanoparticles have been reported to date. The first one is based on the lotus-flower-like SeO<sub>2</sub>-decorated reduced graphene oxide nanocomposite and used for the amperometric determination of quercetin [12]. It should be noted that electrocatalytic effect is also provided by reduced graphene oxide. Furthermore, the nanocomposite synthesis is a multistage time-consuming process. Another sensor consisted of the glassy carbon electrode modified with SeO<sub>2</sub> nanoparticles and hexadecyltriphenylphosphonium bromide has been developed for the sensitive voltammetric quantification of carminic acid in candies [13]. Thus, further development of electrochemical sensors based on the SeO<sub>2</sub> nanoparticles is of practical interest.

Colorants of various classes are widely used in the food, pharmaceutical, and cosmetic industries. Their contents in real samples have to be strictly controlled due to the

dose-dependent negative health effects [14]. The majority of colorants can undergo electroreduction or/and electrooxidation allowing their electrochemical determination which is favorable vs. other methods as they are highly sensitive, simple, reliable, cost-effective, and can be miniaturized and realized outside the laboratory.

The blue colorant indigo carmine (disodium [2(2')E]-3,3'-dioxo-1,1',3,3'-tetrahydro[2,2'-biindolylidene]-5,5'-disulfonate, E132) (Figure 1) is of interest among a wide range of colorants. It is used in the food and pharmaceutical industry [15] as well as in medicine for diagnostic purposes [16]. Nevertheless, the overdose of indigo carmine can lead to side effects in the liver, central nervous system, kidneys, and eyes, as well as show mutagenic effects leading to oncogenesis [17]. Therefore, the acceptable daily intake of  $5.0 \text{ mg kg}^{-1} \text{ d}^{-1}$  is reported for the indigo carmine [17], and its contents in real samples have to be monitored as part of the quality control procedure.

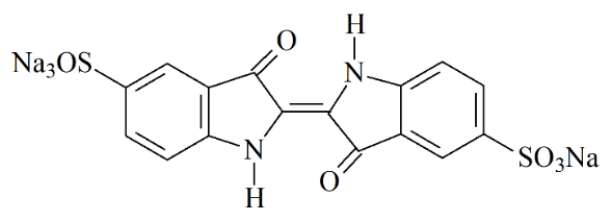


**Figure 1.** Indigo carmine structure.

Indigo carmine is an electroactive colorant able to perform the reduction at the electrode surface with the formation of leucoindigo carmine and to the oxidation to dehydroindigo carmine (Figure 2) [18]. Both processes involve two electrons' and two protons' transfer.

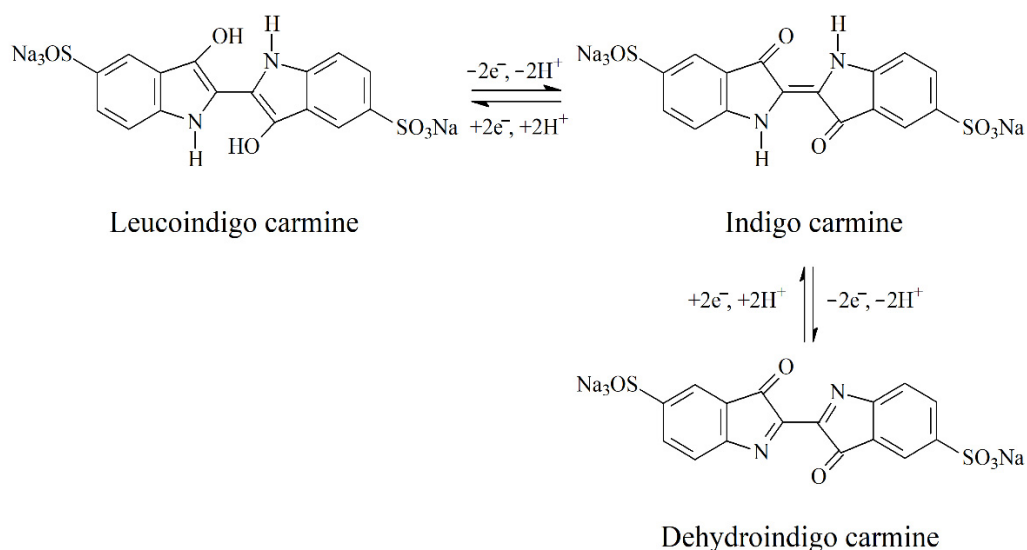


**Figure 2.** Redox behavior of indigo carmine.

The colorant reduction has been studied at the silver-based mercury film [19] and screen-printed [20] electrodes. The oxidation of indigo carmine at the platinum [21], screen-printed carbon [22] electrodes, and cathodically pretreated boron-doped diamond electrode [23,24] has been reported. Recently, a wide range of voltammetric sensors based on 4-(4-nitrophenylazo)N-benzyl,N-ethylaniline [25], electropolymerized arginine [26] and glycine [27], zinc porphyrins and zinc phthalocyanine [28], combination of poly(glutamic acid) [29] and chiral amine bis(phenolate) boron complex with multiwalled carbon nanotubes [30] modified electrodes have been developed for the quantification of indigo carmine. Modification of the electrode surface provides significant improvement in the analytical characteristics of the colorant compared to bare electrodes, although limits of

detection and linear dynamic ranges obtained for alternating current voltammetric and flow-ampereometric detection modes are comparable to the modified electrodes. Other electrochemical sensors with modified surfaces show characteristics comparable to each other that can be further improved. It should be mentioned that there are no data regarding metal and non-metal oxide nanoparticle-based electrochemical sensors for indigo carmine.

The current work is focused on the development of a novel voltammetric sensor for indigo carmine based on the glassy carbon electrode (GCE) modified with SeO<sub>2</sub> nanoparticles and surfactants. The effect of surfactant nature and concentration on the voltammetric characteristics of indigo carmine was studied. SeO<sub>2</sub> nanoparticles dispersed in cationic cetylpyridinium bromide provided the best response. The electrooxidation parameters of the indigo carmine were evaluated using cyclic voltammetry. A highly sensitive voltammetric sensor was developed for colorant quantification and successfully tested on pharmaceutical dosage forms.

## 2. Materials and Methods

### 2.1. Reagents

Indigo carmine of analytical grade was obtained from Sigma-Aldrich (Steinheim, Germany). Its standard 10 mM solution was prepared by dissolving an accurately weighed portion in distilled water. An exact dilution was used for the preparation of less concentrated solutions.

SeO<sub>2</sub> powder of 99.9% purity from Aldrich (Saint Louis, MO, USA) was used. The 1.0 mg mL<sup>-1</sup> homogeneous dispersions of SeO<sub>2</sub> nanoparticles in surfactants aqueous solutions of various concentrations were obtained by sonication for 20 min in WiseClean WUC-A03H ultrasonic bath (DAIHAN Scientific Co., Ltd., Wonju-si, Korea).

Cationic cetylpyridinium bromide (CPB) of 98% purity (Aldrich, Steinheim, Germany) and cetyltrimethylammonium bromide (CTAB) (99% from Acros Organics, Geel, Belgium), anionic sodium dodecyl sulfate (SDS) of Ph. Eur. grade (Panreac, Barcelona, Spain) and N-lauroylsarcosine sodium salt (LSS) (97% from Aldrich, Steinheim, Germany), and non-ionic Brij<sup>®</sup> 35 (Acros Organics, Geel, Belgium) and Triton X-100 from Aldrich (Steinheim, Germany) were used as dispersive agents. Their 1.0 mM standard solutions were prepared by the dissolution of the exact weighed portion of the substance in distilled water.

Ascorbic acid (99% from Sigma, Steinheim, Germany), DL-menthol (95% from Sigma-Aldrich, Steinheim, Germany), aspartame (98% from Sigma-Aldrich, Steinheim, Germany), benzydamine hydrochloride (Sigma-Aldrich, Steinheim, Germany), riboflavin (98% from Sigma-Aldrich, Steinheim, Germany), and quinoline yellow (95% from Acros Organics, Geel, Belgium) were used in the interference study. Their 1.0 mM solutions in water were prepared by dissolution of the accurately weighed portion.

Other reagents were of c.p. grade. Distilled water was used for the measurements. The experiments were carried out at laboratory temperature (25 ± 2 °C).

### 2.2. Apparatus

Potentiostat/galvanostat  $\mu$ Autolab Type III (Eco Chemie B.V., Utrecht, The Netherlands) with GPES 4.9.005 software was used for the voltammetric and chronoamperometric measurements. Electrochemical impedance spectroscopy (EIS) was performed on the potentiostat/galvanostat Autolab PGSTAT 302N with FRA 32M module (Eco Chemie B.V., Utrecht, The Netherlands) and NOVA 1.10.1.9 software. A 10 mL glass electrochemical cell consisted of a glassy carbon electrode (GCE) with 7.07 mm<sup>2</sup> geometric surface area (CH Instruments, Inc., Bee Cave, TX, USA) or SeO<sub>2</sub> nanoparticles modified GCE as working electrode, a silver-silver chloride 3.5 M KCl reference electrode, and a platinum counter electrode was used.

An "Expert-001" pH meter (Econix-Expert Ltd., Moscow, Russia) equipped with the glass electrode was used for pH measurements.

High-resolution field emission scanning electron microscope Merlin™ (Carl Zeiss, Oberkochen, Germany) operated at the 5 kV accelerating voltage and 300 pA emission current was used for the electrode surface characterization.

### 2.3. Procedures

#### 2.3.1. Sensor Fabrication

The GCE was carefully polished with alumina (0.05 μm) on a polishing cloth, rinsed with acetone, and distilled water. Electrode modification was performed by drop-casting of 4 μL of SeO<sub>2</sub> nanoparticles dispersion on the surface of GCE and evaporation to dryness for 15 min at room temperature.

#### 2.3.2. Electrochemical Measurements

Voltammetric measurements were performed in the phosphate buffer (PB) of various pH. After fivefold scanning of the potential in the supporting electrolyte, an aliquot of the indigo carmine solution (5.0–50 μL) was added to the electrochemical cell. Cyclic voltammograms were registered within the potential range of 0.1 to 1.0 V at the scan rate of 100 mV s<sup>-1</sup>. Anodic differential pulse voltammograms were recorded from 0.30 to 0.70 V. The pulse parameters were varied. To calculate the oxidation currents in the differential pulse mode, baseline correction using GPES 4.9.005 software (Eco Chemie B.V., Utrecht, The Netherlands) under the moving average algorithm was used.

Chronoamperometry was performed at a potential of 0.45 V in the presence of 1.0 mM K<sub>4</sub>[Fe(CN)<sub>6</sub>] in 0.1 M KCl. The electrolysis time was 75 s.

Electrochemical impedance spectroscopy was performed in the presence of 1.0 mM K<sub>4</sub>[Fe(CN)<sub>6</sub>]/K<sub>3</sub>Fe(CN)<sub>6</sub> in 0.1 M KCl in the frequency range of 10 kHz–0.04 Hz (9 points per order of magnitude) with an applied sine potential amplitude of 5 mV at a polarization potential of 0.22 V.

Spectrophotometric measurements were performed on the spectrophotometer PE-5300 (NPO Ecros, Saint Petersburg, Russia).

#### 2.3.3. Evaluation of the Electroactive Surface Area of the Electrodes

Cyclic voltammetry and chronoamperometry of 1.0 mM K<sub>4</sub>[Fe(CN)<sub>6</sub>] in 0.1 M KCl were applied for the estimation of electrodes electroactive surface area. Due to the irreversible oxidation of hexacyanoferrate(II) ions on GCE, chronoamperometric data and Cottrell equation [31] (Equation (1)) were used.

$$I = nFAcD^{\frac{1}{2}}\pi^{-\frac{1}{2}}t^{-\frac{1}{2}}, \quad (1)$$

where  $I$  is the current (A),  $n$ —the number of transferred electrons,  $F$ —the Faraday constant (C mol<sup>-1</sup>),  $A$ —the electrode surface area (cm<sup>2</sup>),  $c$ —concentration (mol cm<sup>-3</sup>),  $D$ —diffusion coefficient (cm<sup>2</sup> s<sup>-1</sup>) and  $t$ —the electrolysis time (s). For 1.0 mM K<sub>4</sub>[Fe(CN)<sub>6</sub>] in 0.1 M KCl,  $n = 1$  and  $D = 7.6 \times 10^{-6}$  cm<sup>2</sup> s<sup>-1</sup> at 298 K.

Electroactive surface area of the SeO<sub>2</sub> nanoparticles modified GCE was calculated using cyclic voltammetry data and Randles-Sevcik equation [31] (Equation (2)) as far as a reversible oxidation of redox probe was observed.

$$I_p = \pi^{\frac{1}{2}}\chi_p n^{\frac{3}{2}} F^{\frac{3}{2}} A c D^{\frac{1}{2}} (RT)^{-\frac{1}{2}} \nu^{\frac{1}{2}}, \quad (2)$$

where  $I_p$  is a peak current (A),  $\chi_p$ —normalized current for sweep experiments with a reversible system,  $R$ —the universal gas constant (J mol<sup>-1</sup> K<sup>-1</sup>),  $T$ —temperature (K) and  $\nu$ —potential scan rate (V s<sup>-1</sup>). Other variables had the same meaning as in Equation (1).

#### 2.3.4. Pharmaceutical Dosage Forms Analysis

Commercially available pharmaceutical dosage forms containing indigo carmine as colorant (vitamin tablets, lozenges for symptomatic local treatment for the relief of pain

and irritation of the mouth and throat, and capsules of non-steroidal anti-inflammatory drug) were used as real samples. The average mass of lozenges, tablets, or capsules shells was preliminarily measured. Then, five lozenges, tablets, or capsules shells of known mass were dissolved in distilled water using a 50 mL flask. In the case of the vitamin tablets, the solution was filtered after the full dissolving of the tablets' coverage containing the colorant.

PB pH 5.0 was placed into the electrochemical cell and five differential pulse voltammograms were recorded. Then, an aliquot portion of the sample solution (50–150  $\mu\text{L}$ ) was added and differential pulse voltammograms were registered from 0.30 to 0.70 V at a modulation amplitude of 100 mV, a modulation time of 25 ms, and a potential scan rate of 10  $\text{mV s}^{-1}$ .

Spectrophotometric measurements were performed in 2 cm cuvettes at 610 nm vs. distilled water using a standard addition method.

### 2.3.5. Statistical Treatment of the Data

The measurement results were statistically treated for five replicates at a confidence level of 0.95. All data were expressed as the  $X \pm \Delta X$  with  $X$  as average value and  $\Delta X$  as coverage interval.  $F$ - and  $t$ -tests were used for the validation of the developed and independent methods.

The detection and quantification limits were calculated as  $3SD_a/b$  and  $10SD_a/b$ , respectively, where  $SD_a$  was the standard deviation of the calibration graph intercept and  $b$ —the calibration graph slope.

Regression analysis was performed using the OriginPro 8.1 software (OriginLab, Northampton, MA, USA).

## 3. Results

### 3.1. Voltammetric Characteristics of Indigo Carmine at the Bare and $\text{SeO}_2$ -Nanoparticle-Modified Electrodes

Indigo carmine has shown an irreversible weakly pronounced oxidation step at 0.78 V in PB pH 7.0 at the bare GCE (Figure 3, curve 2). The oxidation currents of  $76 \pm 3$  nA for 50  $\mu\text{M}$  concentration indicate a low sensitivity of the response and its inapplicability to the analytical purposes. To solve this problem, electrode surface modification with  $\text{SeO}_2$  nanoparticles was used.

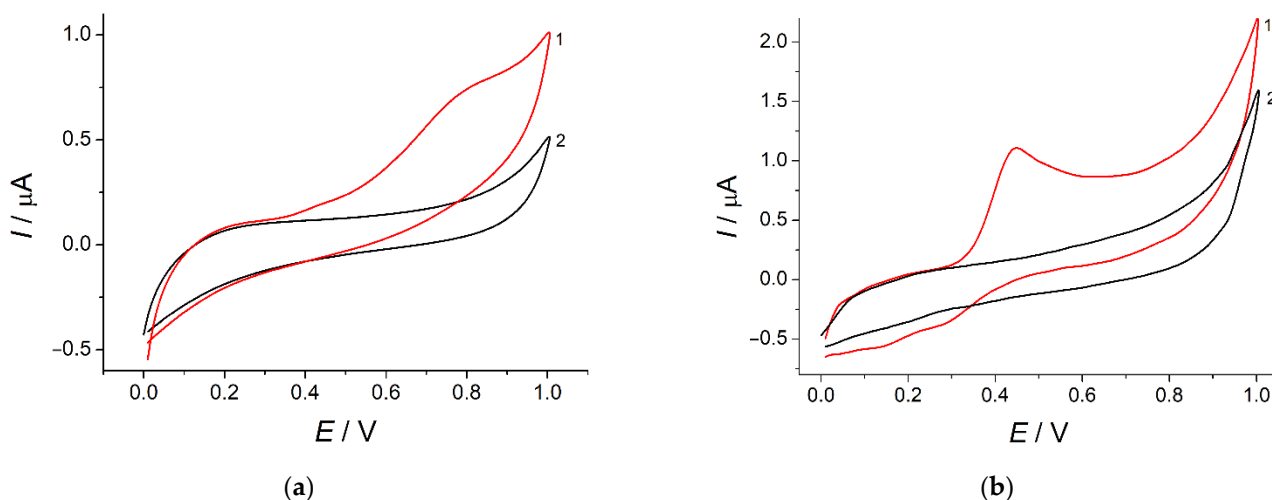


**Figure 3.** Cyclic voltammograms of 50  $\mu\text{M}$  indigo carmine (curve 1) in PB pH 7.0 (curve 2): (a) bare GCE; (b)  $\text{SeO}_2$ -CPB/GCE. Potential scan rate is 100  $\text{mV s}^{-1}$ .

The application of surfactants as dispersive agents and stabilizers for nanoparticles dispersion preparation has been successfully shown for electrochemically inert metal oxide nanoparticles such as  $\text{CeO}_2$  [32,33] and  $\text{SnO}_2$  [34,35]. Furthermore, surfactants act

as electrode surface co-modifiers providing organic compounds preconcentration at the electrode surface [36–39]. The mechanism of surfactant–analyte interactions can vary depending on the nature of both compounds. Thus, dispersions of  $\text{SeO}_2$  particles in surfactant media of various nature and concentrations were used.  $\text{SeO}_2$  nanoparticles are formed in the dispersion and act as electrode surface modifier as scanning electron microscopy confirms (see Section 3.2). Similar behavior has been reported for the  $\text{SiO}_2$  nanoparticles [13,40].

The effect of surfactants' nature and concentration in the  $\text{SeO}_2$  nanoparticles dispersion on the voltammetric behavior of indigo carmine was studied under conditions of cyclic voltammetry. Cationic (CPB and CTAB), anionic (SDS and LSS), and nonionic surfactants (Brij® 35 and Triton X-100) in the concentration range of 0.050–1.0 mM were used. The changes of indigo carmine voltammetric characteristics are presented in Figure 4. The oxidation potential is significantly decreased as the surfactant concentration increases independently of the surfactant type (Figure 4a). This means the increase in the electron transfer rate for the modified electrodes due to the presence of surfactant. The only exclusion is Triton X-100 for which almost no effect is observed that is probably caused by the presence of polyethylene oxide chain in surfactant structure affecting interaction with the analyte. The oxidation currents of indigo carmine are changed in different ways depending on the surfactants' nature (Figure 4b).

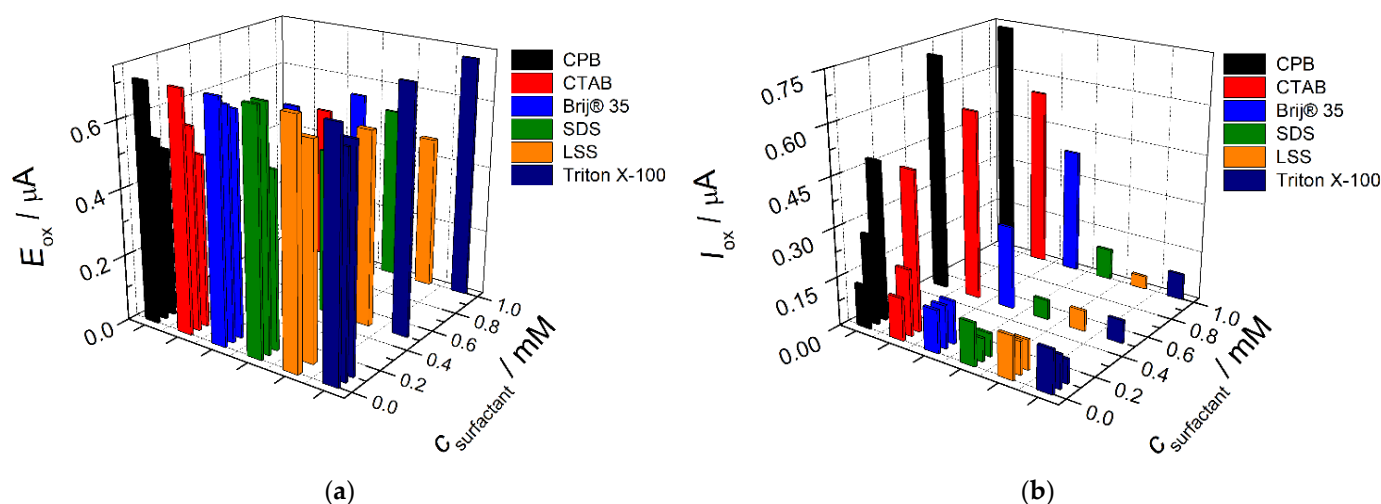


**Figure 4.** Effect of surfactants on the voltammetric characteristics of 50 μM indigo carmine at the  $\text{SeO}_2$ –Surfactant/GCE: (a) effect on the oxidation potential; (b) effect on the oxidation currents. Supporting electrolyte is 0.1 M phosphate buffer, pH 7.0.

Anionic SDS and LSS significantly depress the oxidation peak in the whole concentration range that is explained by electrostatic repulsion between negatively charged at pH 7.0 surfactant and indigo carmine. Non-ionic surfactants show a different effect on the indigo carmine oxidation currents. Brij® 35 up to 0.10 mM level does not affect the indigo carmine response while 0.50–1.0 mM concentration of surfactant leads to the increase in the colorant oxidation current. Triton X-100 shows similar to anionic surfactants effect, i.e., significant decrease in the indigo carmine oxidation currents. Cationic surfactants in the whole concentration range provide a statistically significant (1.6–5.7-fold) increase in the oxidation currents of indigo carmine vs. those at the bare GCE. The data obtained allow to conclude that electrostatic interactions play a major role in the carminic acid response. As shown on cationic CPB and CTAB, the hydrophobic interactions also contribute to the improvement in the voltammetric characteristics of indigo carmine. The more pronounced effect in the case of CPB can be explained by the possibility of  $\pi$ – $\pi$  stacking between the aromatic rings of surfactant and indigo carmine molecules.

The best response of indigo carmine was registered at the electrode modified with  $\text{SeO}_2$  nanoparticles dispersed in 1.0 mM CPB (Figure 1, curve 3) that was used in further investigations. The increase in the oxidation currents is caused by the increase in the effective surface area of the modified electrode (Section 3.2) as well as preconcentration of the colorant at the electrode surface via electrostatic and hydrophobic interactions with a surfactant as confirmed in further investigations (Section 3.3). Furthermore, two worse pronounced reduction steps are appeared in the case of modified electrode that means the improvement in the electrochemical system reversibility.

It should be noted that the synergetic effect of both  $\text{SeO}_2$  nanoparticles and CPB provides an excellent response of the electrode towards indigo carmine. This suggestion is confirmed by the application of CPB-modified electrode providing approximately a 2.0-fold increase in indigo carmine oxidation currents. Furthermore, the reproducibility of the electrode response is insufficient due to the possibility of partial leaching of CPB from the electrode surface after insert in the supporting electrolyte.

### 3.2. Microscopic and Electrochemical Characterization of the Electrodes

Scanning electron microscopy was applied for the characterization of GCE and  $\text{SeO}_2$ -CPB/GCE surface (Figure 5). Bare GCE demonstrates a relatively smooth surface of insignificant roughness (Figure 5a).  $\text{SeO}_2$  nanoparticles dispersed in 1.0 mM CPB form porous coverage with the spheroid particles of 39–55 nm that are uniformly distributed at the GCE surface (Figure 5b). Microscopic data confirm the successful immobilization of  $\text{SeO}_2$  nanoparticles at the GCE surface.

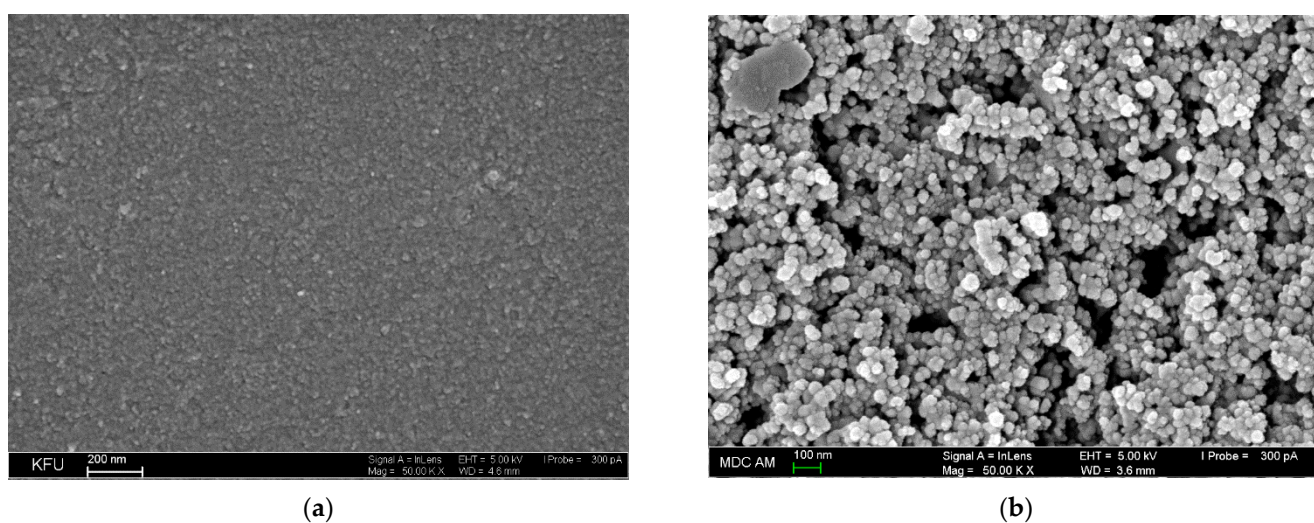


**Figure 5.** Electrodes surface morphology obtained by scanning electron microscopy: (a) bare GCE; (b)  $\text{SeO}_2$ -CPB/GCE.

The electrode surface modification leads to the increase in the surface area due to the porous structure. The electroactive surface area is also 4.2-fold increased vs. bare GCE ( $37.4 \pm 0.2$  vs.  $8.9 \pm 0.2$   $\text{mm}^2$ , respectively) as confirmed by electrochemical data for the electrooxidation of hexacyanoferrate(II) ions in 0.1 M KCl. Furthermore, the application of  $\text{SeO}_2$  nanoparticles dispersion in CPB as electrode surface modifier provides significant improvement in the redox probe system reversibility (Figure 6a, curve 3) vs. bare GCE that indicates the increase in the electron transfer rate on the modified electrode. These data are fully coincided with electrochemical impedance spectroscopy investigation (Figure 6b).

A dramatic decrease in the semicircle diameter in the high frequencies region for the modified electrode indicates significant improvement in the electron transfer vs. GCE. This is also confirmed by electrochemical spectra fitting (Table 1) using Randles equivalent cell consisting of electrolyte resistance ( $R_s$ ), constant phase element ( $Q$ ), charge transfer

resistance ( $R_{ct}$ ) and Warburg impedance ( $W$ ) [41]. Charge transfer resistance for the modified electrode is 5043-fold lower than for bare GCE that means increase in the electron transfer rate. The constant phase element value for  $\text{SeO}_2$ -nanoparticle-modified electrode is 26.3-fold higher than for bare GCE that can be explained by the increase in the electrode surface total charge due to the presence of CPB. Fitting error ( $\chi^2$  parameter) does not exceed 0.04 confirming accuracy of the equivalent electrical circuit applied. Thus, electrochemical data confirm effectivity of  $\text{SeO}_2$  nanoparticles dispersion in CPB as a novel type of the electrode surface modifiers for the creation of electrochemical sensors.

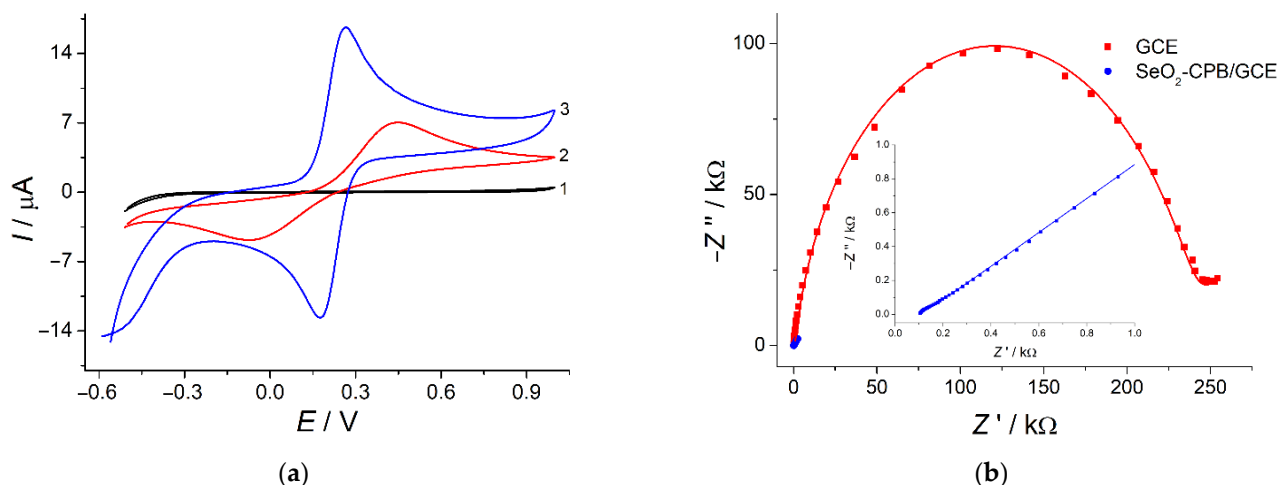


**Figure 6.** (a) Cyclic voltammograms for 1.0 mM  $[\text{Fe}(\text{CN})_6]^{4-}$  at the bare GCE (curve 2) and  $\text{SeO}_2$ -CPB/GCE (curve 3) in 0.1 M KCl (curve 1), potential scan rate is  $100 \text{ mV s}^{-1}$ ; (b) Experimental (points) and fitted (lines) Nyquist plots for bare GCE and  $\text{SeO}_2$ -CPB/GCE in the presence of 1.0 mM  $[\text{Fe}(\text{CN})_6]^{4-}/3-$  in 0.1 M KCl.  $E = 0.22 \text{ V}$ ; frequency range, 10 kHz—0.04 Hz; amplitude, 5 mV.

**Table 1.** Electrochemical impedance parameters of the electrodes ( $n = 5$ ;  $p = 0.95$ ).

Electrode	$R_s$ ( $\Omega$ )	$R_{ct}$ ( $\text{k}\Omega$ )	$Q$ ( $\mu\Omega^{-1}$ )	$n$	$W$ ( $\mu\Omega^{-1}$ )	$\chi^2$
GCE	$93 \pm 3$	$232 \pm 7$	$0.198 \pm 0.003$	0.898	$62 \pm 3$	0.040
$\text{SeO}_2$ -CPB/GCE	$104 \pm 5$	$0.046 \pm 0.005$	$5.2 \pm 0.3$	0.936	$394 \pm 6$	0.032

### 3.3. Indigo Carmine Electrooxidation Parameters

Electrochemical oxidation of indigo carmine at the  $\text{SeO}_2$ -CPB/GCE and quantitative characteristics of the process were evaluated using cyclic voltammetry. Firstly, the effect of phosphate buffer pH in the range of 4.5–8.0 on the voltametric characteristics of colorant was studied (Figure 7).

Oxidation of indigo carmine proceeds irreversibly in the whole pH range. There are two weak reduction steps on the cyclic voltammograms at the 4.5–7.0 pH. In spite of the presence of reduction steps on the cathodic branches of voltammograms, indigo carmine oxidation is irreversible as far as the redox peak potential separation is close to 150 mV and currents ratio is significantly less than 1.0. Colorant oxidation/reduction potentials are cathodically shifted with the increase in the phosphate buffer pH. Thus, protons participate in the indigo carmine electrooxidation. The anodic currents at pH 4.5 and 5.0 are the same and then start to decrease as pH is grown. Reduction currents are gradually decreased with the pH increase up to their full disappearance in a basic medium. Phosphate buffer of pH 5.0 has been chosen for further investigations as it provides the highest oxidation currents of indigo carmine and their better reproducibility in comparison to pH 4.5.

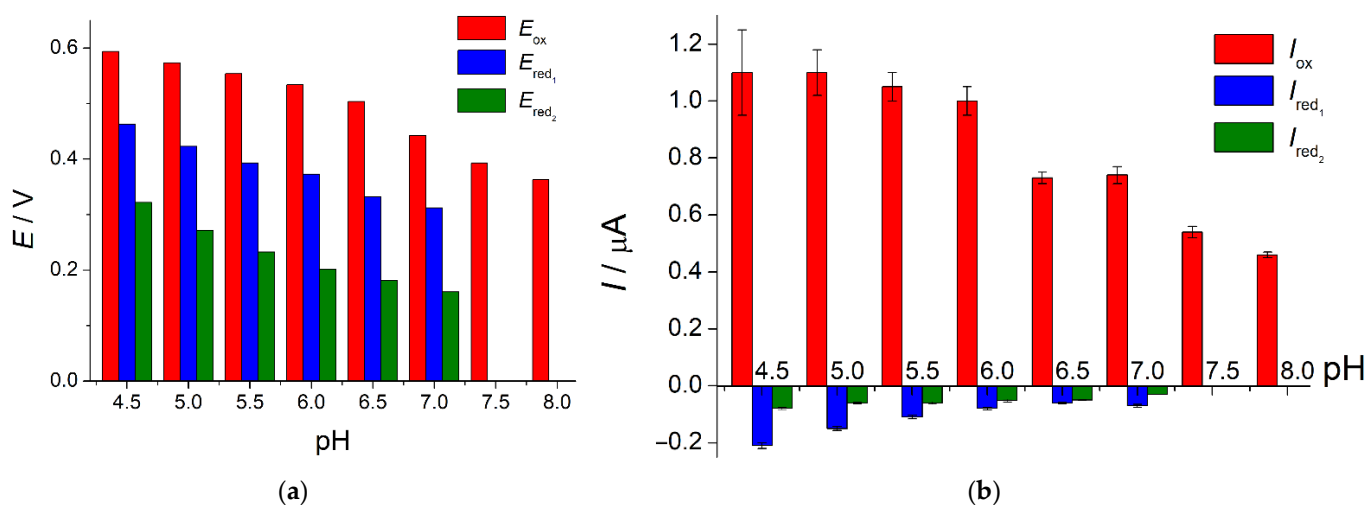


**Figure 7.** Effect of phosphate buffer pH on the voltammetric characteristics of 50 μM indigo carmine at the SeO<sub>2</sub>-CPB/GCE: (a) the changes of the oxidation potential; (b) the changes of the oxidation currents.

The effect of potential scan rate in the range of 5–150 mV s<sup>-1</sup> on the voltammetric response of indigo carmine was evaluated (Figure 8). There is a well-defined oxidation peak of indigo carmine at 0.574 V which is insignificantly increased with the potential scan rate growth.

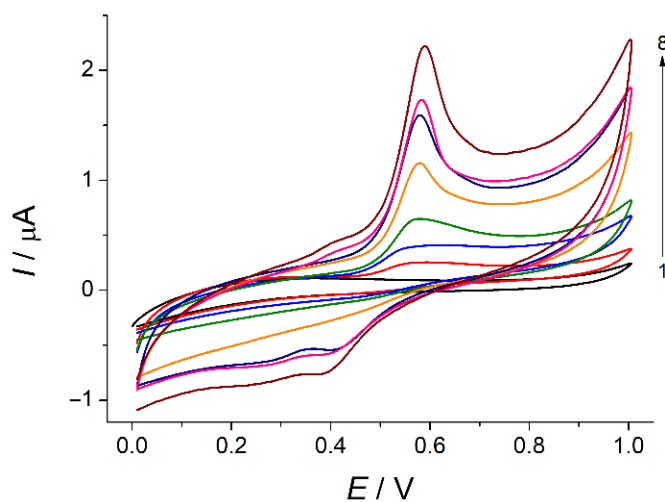


**Figure 8.** Cyclic voltammograms of 50 μM indigo carmine at the SeO<sub>2</sub>-CPB/GCE at the various potential scan rates: 5 (curve 2), 10 (3), 25 (4), 50 (5), 75 (6), 100 (7), and 150 (8) mV s<sup>-1</sup> in phosphate buffer pH 5.0 (curve 1).

The peak currents are linearly increased with the potential scan rate in the range of 5–75 mV s<sup>-1</sup> (Equation (3), Figure S1a) and the slope of the plot  $\ln I = f(\ln \nu)$  is close to 1.0 (Equation (4), Figure S1b) that confirms the surface-controlled electrooxidation. Similar behavior has been reported for polyarginine- [26] and polyglycine-modified [27] carbon paste electrodes. Further increase in the scan rate leads to the deviation from linearity that is also typical for the surface-controlled processes. Thus, the data obtained confirms preconcentration of indigo carmine at the electrode surface due to the interaction with CPB.

$$I_p [\mu\text{A}] = (0.025 \pm 0.002) + (0.0134 \pm 0.0005) \nu [\text{mV s}^{-1}] R^2 = 0.99995, \quad (3)$$

$$\ln I_p [\mu\text{A}] = (2.38 \pm 0.07) + (0.91 \pm 0.02) \ln \nu [\text{V s}^{-1}] R^2 = 0.99855, \quad (4)$$

The electrooxidation parameters of indigo carmine have been found. The  $\alpha_a n$  of 1.01 has been calculated from Equation (5) [31].

$$\Delta E_{1/2} = 62.5 / \alpha_a n, \quad (5)$$

The anodic transfer coefficient  $\alpha_a = 0.46$  has been calculated using Equation (6) [31].

$$I_p = \frac{\alpha_a n \alpha F Q v}{2.718 RT}, \quad (6)$$

Thus, the number of electrons participating in the indigo carmine electrooxidations equals to two. Based on the data obtained, the two electron and two proton irreversible electrochemical process with formation of dehydroindigo carmine is suggested that agree well to be reported for other modified electrodes [25–27].

Equation (7) has been applied for the calculation of the indigo carmine surface coverage ( $\Gamma$ ) [31].

$$I_p = \frac{n \alpha_a n \alpha F^2 A v \Gamma}{2.718 RT}, \quad (7)$$

Indigo carmine surface coverage is  $(1.8 \pm 0.1) \times 10^{-10} \text{ mol cm}^{-2}$ .

### 3.4. Indigo Carmine Sensing Using $\text{SeO}_2$ Nanoparticles Modified Electrode

The electrode developed was applied as a voltammetric sensor for indigo carmine. A differential pulse voltammetry was chosen for the improvement in the colorant response sensitivity. The changes of the pulse parameters have shown that the best parameters of the indigo carmine analytical signal are achieved using pulse width of 0.10 V and pulse height of 0.025 s (Figure 9).

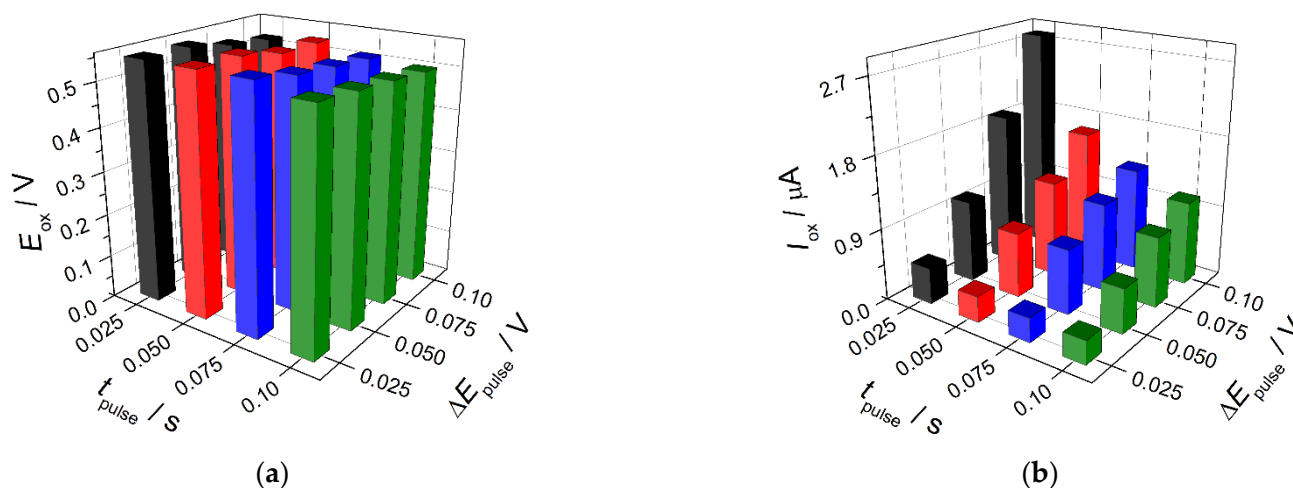


**Figure 9.** Effect of pulse parameters on the voltammetric characteristics of 50  $\mu\text{M}$  indigo carmine at the  $\text{SeO}_2$ -CPB/GCE in phosphate buffer pH 5.0: (a) the changes of the oxidation potential; (b) the changes of the oxidation currents.

Under these conditions, the sensor gives well-resolved response to indigo carmine at 0.47 V (Figure 10).

The oxidation currents are linearly dependent on the colorant concentration in the ranges of 0.025–1.0 (Equation (8), Figure S2a) and 1.0–10  $\mu\text{M}$  (Equation (9), Figure S2b) with the detection and quantification limits of 4.3 and 14.3 nM, respectively.

$$I [\mu\text{A}] = (-0.0089 \pm 0.008) + (55.9 \pm 0.2) \times 10^4 c [\text{M}] R^2 = 0.99994, \quad (8)$$

$$I [\mu\text{A}] = (0.417 \pm 0.006) + (127.9 \pm 0.9) \times 10^3 c [\text{M}] R^2 = 0.99979, \quad (9)$$

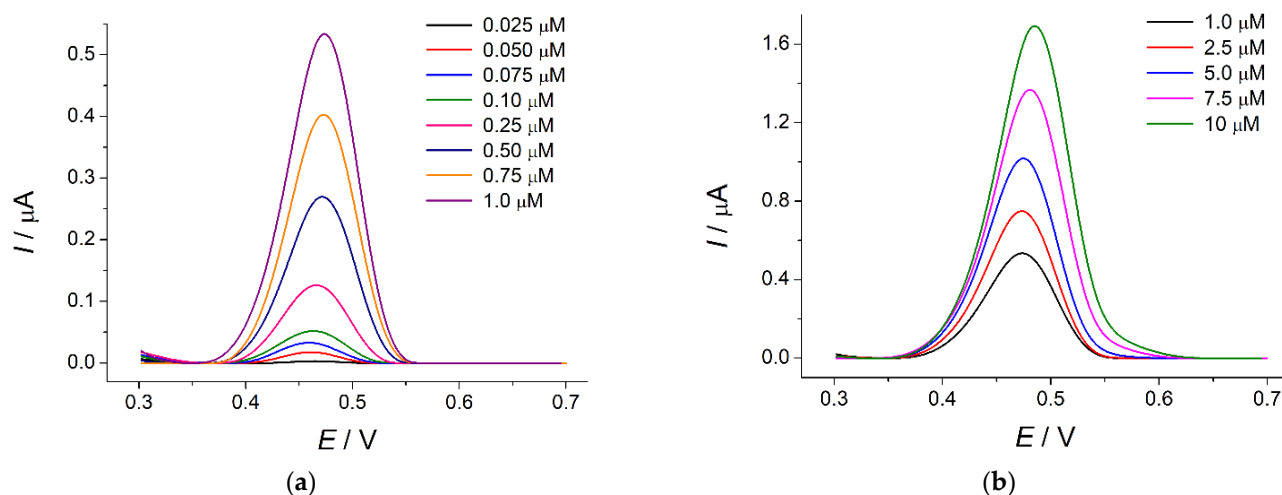


**Figure 10.** Baseline-corrected differential pulse voltammograms of indigo carmine at the  $\text{SeO}_2$ -CPB/GCE in phosphate buffer pH 5.0: (a) 0.025–1.0  $\mu\text{M}$ ; (b) 1.0–10  $\mu\text{M}$ . Pulse width is 0.10 V, pulse height is 0.025 s, and potential scan rate is 10  $\text{mV s}^{-1}$ .

The calibration graph slopes indicate the high sensitivity of the sensor developed. The obtained analytical characteristics of indigo carmine are among the best ones reported to date (Table 2).

**Table 2.** Figures of merit for the electrochemical sensors for indigo carmine.

Sensor	Detection Mode	Limit of Detection ( $\mu\text{M}$ )	Linear Dynamic Range ( $\mu\text{M}$ )	Ref.
Silver-based mercury film electrode	AdSV <sup>1</sup>	-	0–0.21	[19]
Screen-printed electrode	Flow amperometry	0.033	0.05–100	[20]
Screen-printed carbon electrodes	CV <sup>2</sup>	0.19	0.5–100	[22]
	DPV <sup>3</sup>	0.17	0.2–20	
	SWV <sup>4</sup>	0.34	0.7–10	
	ACV <sup>5</sup>	0.032	0.06–0.7	
Cathodically pretreated boron-doped diamond electrode	SWV	0.058	0.5–84.1	[23]
4-(4-Nitrophenylazo)N-benzyl,N-ethylaniline—CPE <sup>7</sup>	FIA-MPA <sup>6</sup>	0.040	0.07–1.0	[24]
Polyarginine/CPE	DPV	0.36	1–100	[25]
Polyglycine/CPE	DPV	0.0253	0.2–1.0 and 1.5–3.5	[26]
Zinc tetraphenylporphyrin—Graphite PDM <sup>8</sup>	CV	0.011	2–10 and 15–60	[27]
Zinc tetranaphthoporphyrin—Graphite PDM		$3.87 \times 10^{-8}$	$1.00 \times 10^{-6}$ – $1.00 \times 10^{-4}$	
Zinc tetrasulphophenylporphyrin—Graphite PDM		$2.30 \times 10^{-6}$	$1.00 \times 10^{-4}$ – $1.00 \times 10^{-2}$	
Zinc phthalocyanine—Graphite PDM		$1.65 \times 10^{-6}$	$1.00 \times 10^{-6}$ – $1.00 \times 10^{-4}$	
Zinc tetraphenylporphyrin—Diamond PDM	DPV	$4.26 \times 10^{-5}$	$1.00 \times 10^{-3}$ – $1.00 \times 10^{-1}$	[28]
Zinc tetranaphthoporphyrin—Diamond PDM		0.0796	0.010–10	
Zinc tetrasulphophenylporphyrin—PDM		$1.20 \times 10^{-5}$	$1.00 \times 10^{-4}$ – $1.00 \times 10^{-2}$	
Zinc phthalocyanine—Diamond PDM		0.0012	0.010–10	
Poly(glutamic acid)/MWNT <sup>9</sup> -based paste electrode	DPV	0.0333	0.010–1.0	
Chiral amine bis(phenolate) boron complex containing N,N-diethyl-p-phenylenediamine—carboxylated MWNT/GCE	DPV	0.36	5.0–50	[29]
	SWV	0.019	0.1–30	[30]
$\text{SeO}_2$ nanoparticles—CPB/GCE	DPV	0.0043	0.025–1.0 1.0–10	Current

<sup>1</sup> Adsorptive stripping voltammetry. <sup>2</sup> Cyclic voltammetry. <sup>3</sup> Differential pulse voltammetry. <sup>4</sup> Square-wave voltammetry. <sup>5</sup> Alternating current voltammetry. <sup>6</sup> Flow injection analysis with multiple pulse amperometric detection. <sup>7</sup> Carbon paste electrode. <sup>8</sup> Paste dot microsensor. <sup>9</sup> Multi-walled carbon nanotubes.

The most impressive characteristics for the trace analysis of indigo carmine were obtained at the graphite and diamond paste dot microsensors modified with zinc porphyrins and phthalocyanine [28]. Nevertheless, the modifier can show an electrocatalytic effect to a wide range of compounds contained in the real samples. The selectivity test covers only alizarin red and alizarin blue while other synthetic colorants with the related structure and

typical constituents are out of consideration. The practical applicability of the sensors was shown on the spiked wastewater only.

Another advantage of the sensor developed is a simple one-step fabrication as well as easy and express preparation of the modifier.

The sensor response is of high accuracy (99–100%) and reproducibility (RSD values of 0.65–2.1%) that is shown on the indigo carmine model solutions (Table 3). The indigo carmine electrooxidation product is adsorbed at the sensor surface leading to significant decrease (30–50%) in the colorant oxidation currents. Therefore, sensor surface renewal is required after each measurement. On the other hand, the single usable screen-printed electrodes based on the modifier developed can be fabricated.

**Table 3.** Indigo carmine determination in model solutions ( $n = 5$ ;  $p = 0.95$ ).

Added ( $\mu\text{g}$ )	Oxidation Current ( $\mu\text{A}$ )	Found ( $\mu\text{g}$ )	RSD (%)	Recovery (%)
0.0583	$0.005 \pm 0.0002$	$0.058 \pm 0.001$	1.0	$99 \pm 1$
0.233	$0.046 \pm 0.002$	$0.23 \pm 0.01$	1.8	$100 \pm 2$
1.75	$0.41 \pm 0.01$	$1.74 \pm 0.03$	1.3	$99 \pm 2$
11.7	$1.06 \pm 0.03$	$11.7 \pm 0.3$	2.1	$100 \pm 2$
23.3	$1.7 \pm 0.03$	$23.3 \pm 0.2$	0.65	$99.8 \pm 0.8$

The sensor response robustness was evaluated by changing reference and working electrodes, orthophosphoric acid and sodium hydroxide used for the phosphate buffer preparation, dispersion of  $\text{SeO}_2$  nanoparticles in CPB as sensor surface modifier. The RSD values of the oxidation currents of  $0.50 \mu\text{M}$  indigo carmine does not exceed 2.5% confirming high robustness of the developed sensor response.

The selectivity of indigo carmine response was studied at the  $0.50 \mu\text{M}$  level. The most typical interferences such as inorganic ions (1000-fold excess of  $\text{K}^+$ ,  $\text{Mg}^{2+}$ ,  $\text{Ca}^{2+}$ ,  $\text{NO}_3^-$ ,  $\text{Cl}^-$  and  $\text{SO}_4^{2-}$  ions) and saccharides (100-fold excess of glucose, sucrose, rhamnose) are electrochemically inactive in the potential range under consideration and do not affect indigo carmine response. Ascorbic acid is oxidized at 0.16 V and does not show interference effect up to  $10 \mu\text{M}$ . Pharmaceutical dosage forms containing indigo carmine as a colorant contain other active and auxiliary principles that can affect the sensor response. Menthol, aspartame, benzydamine hydrochloride, and riboflavin do not oxidize under conditions of the experiment and do not show interference effect. Indigo carmine is often used together with quinoline yellow; therefore, it was tested as a potential interference. Quinoline yellow does not show the oxidation step in the potential range under consideration. Thus, the  $\text{SeO}_2$ -nanoparticle-based sensor shows an excellent selectivity towards indigo carmine.

### 3.5. Application of the Sensor in Pharmaceutical Analysis

The sensor developed was applied for the quantification of indigo carmine in various pharmaceutical dosage forms (vitamin tablets, lozenges for symptomatic local treatment of the mouth and throat, and capsules of non-steroidal anti-inflammatory drug). All samples show a well-defined oxidation peak at 0.47 V corresponding to indigo carmine that is also confirmed by the standard addition method (Figure 11). The recovery values of 99.3–100% (Table 4) indicate the absence of the matrix effects in the pharmaceutical dosage forms analysis.

Indigo carmine quantification results using a  $\text{SeO}_2$ -nanoparticle-based sensor and an independent spectrophotometric method are presented in Table 5. The results of both methods agree with each other as well as with the labelled amount. *t*- and *F*-tests are less than critical, which confirms the absence of systematic errors in the determination and uniform precision of both methods.

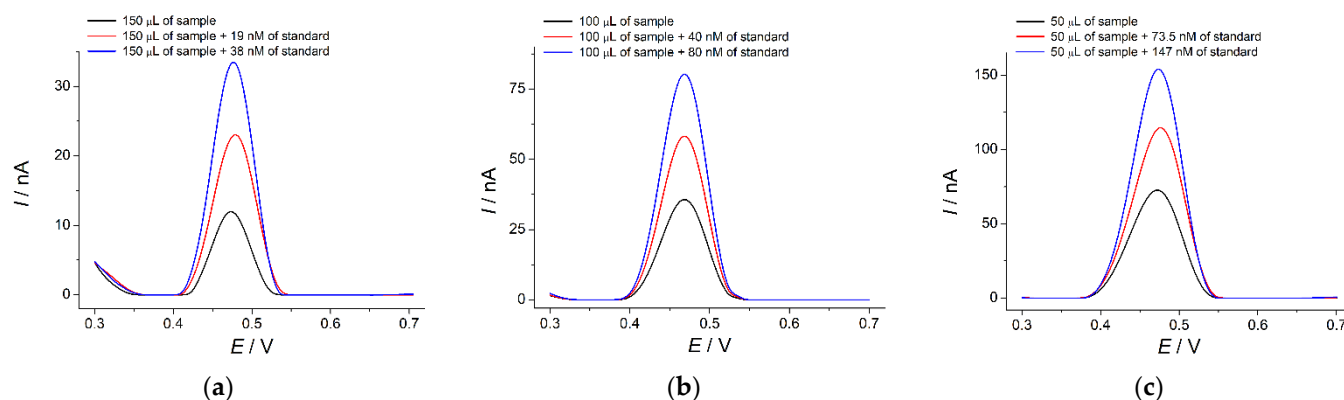


**Figure 11.** Baseline-corrected differential pulse voltammograms of pharmaceutical dosage forms in the absence and in the presence of indigo carmine additions at the  $\text{SeO}_2\text{-CPB/GCE}$  in phosphate buffer pH 5.0: (a) vitamin tablets; (b) lozenges for symptomatic local treatment of the mouth and throat; (c) capsules shell of non-steroidal anti-inflammatory drug. Pulse width is 0.10 V, pulse height is 0.025 s, and potential scan rate is  $10 \text{ mV s}^{-1}$ .

**Table 4.** Indigo carmine recovery in pharmaceutical dosage forms ( $n = 5$ ;  $p = 0.95$ ).

Sample	Spiked (nM)	Found (nM)	RSD (%)	Recovery (%)
Vitamin tablets	0	$38 \pm 2$	3.9	
	19	$57 \pm 2$	2.4	100
	38	$76 \pm 1$	1.5	100
Lozenges	0	$80 \pm 2$	1.9	
	40	$120 \pm 3$	2.4	100
	80	$159 \pm 3$	0.72	99.4
Capsules	0	$147 \pm 7$	3.8	
	73.5	$219 \pm 8$	1.4	99.3
	147	$292 \pm 8$	1.8	99.3

**Table 5.** Quantification of indigo carmine in pharmaceutical dosage forms ( $n = 5$ ;  $p = 0.95$ ).

Sample Type	$N^{\circ}$	Labelled Amount (mg)	Found by Voltammetry (mg)	RSD (%)	Found by Spectrophotometry (mg)	RSD (%)	$t\text{-Test}^1$	$F\text{-Test}^2$
Vitamin tablets		-	$0.0047 \pm 0.0003$	4.4	$0.0051 \pm 0.0003$	4.5	1.97	1.21
Lozenges	1	0.015	$0.0150 \pm 0.0004$	2.3	$0.0148 \pm 0.0003$	1.5	0.976	2.07
	2	0.031	$0.0311 \pm 0.0009$	2.3	$0.0313 \pm 0.0009$	2.4	0.559	1.12
Capsules		-	$0.055 \pm 0.002$	3.7	$0.053 \pm 0.002$	2.7	1.31	0.810

<sup>1</sup>  $t_{\text{crit}} = 2.31$  at  $\alpha = 0.05$  and  $f = 8$ . <sup>2</sup>  $F_{\text{crit}} = 6.39$  at  $\alpha = 0.05$  and  $f_1 = f_2 = 4$ .

#### 4. Conclusions

A novel highly sensitive voltammetric sensor was developed for indigo carmine quantification.  $\text{SeO}_2$  nanoparticles dispersed in cationic surfactant CPB was used as a sensitive layer for the first time. A dual role of CPB as dispersive agent for  $\text{SeO}_2$  nanoparticles and sensor surface co-modifier providing preconcentration of indigo carmine was shown. Such an approach to the sensor surface modification provided high electroactive area and improvement in the electron transfer rate, as well as sufficient conductivity of the sensor.

The analytical characteristics of indigo carmine on the sensor developed are among the best ones reported to date for other electrochemical approaches. Furthermore, the sensor is simple in fabrication and gives a selective, reproducible, robust, and reliable response to indigo carmine. The possibility of the direct analysis of indigo carmine in different

types of pharmaceutical dosage forms using the sensor developed confirms its versatility. The results obtained significantly expand the analytical capabilities of the electrochemical sensors in pharmaceutical quality control.

**Supplementary Materials:** The following are available online at <https://www.mdpi.com/article/10.3390/s22093224/s1>, Figure S1. Effect of potential scan rate on the oxidation currents of 50  $\mu\text{M}$  indigo carmine at the  $\text{SeO}_2\text{-CPB/GCE}$  in phosphate buffer pH 5.0: (a) Plot of oxidation current vs. potential scan rate; (b) Plot of the Napierian logarithm of oxidation current vs. Napierian logarithm of the potential scan rate, Figure S2. Calibration plots of indigo carmine at the  $\text{SeO}_2\text{-CPB/GCE}$  in phosphate buffer pH 5.0: (a) in the concentration range of 0.025–1.0  $\mu\text{M}$ ; (b) in the concentration range of 1.0–10  $\mu\text{M}$ .

**Author Contributions:** Conceptualization, G.Z.; methodology, G.Z. and L.K.; validation, G.Z.; formal analysis, G.Z. and L.K.; investigation, G.Z. and L.K.; writing—original draft preparation, G.Z.; writing—review and editing, G.Z.; visualization, G.Z. and L.K.; supervision, G.Z. All authors have read and agreed to the published version of the manuscript.

**Funding:** This research received no external funding.

**Institutional Review Board Statement:** Not applicable.

**Informed Consent Statement:** Not applicable.

**Data Availability Statement:** The data presented in this study are available in the electronic Supplementary Materials.

**Acknowledgments:** This paper has been supported by the Kazan Federal University Strategic Academic Leadership Program ('PRIORITY-2030'). The authors thank Aleksei Rogov (Laboratory of the Scanning Electron Microscopy, Interdisciplinary Center for Analytical Microscopy, Kazan Federal University) for the scanning electron microscopy measurements.

**Conflicts of Interest:** The authors declare no conflict of interest.

## References

1. Sabeela, N.I.; Almutairi, T.M.; Al-Lohedan, H.A.; Ezzat, A.O.; Atta, A.M. Reactive mesoporous pH-sensitive amino-functionalized silica nanoparticles for efficient removal of coomassie blue dye. *Nanomaterials* **2019**, *9*, 1721. [[CrossRef](#)] [[PubMed](#)]
2. Hamdi, K.; Hébrant, M.; Martin, P.; Galland, B.; Etienne, M. Mesoporous silica nanoparticle film as sorbent for in situ and real-time monitoring of volatile BTX (benzene, toluene and xylenes). *Sens. Actuators B* **2016**, *223*, 904–913. [[CrossRef](#)]
3. Darwish, G.H.; Asselin, J.; Tran, M.V.; Gupta, R.; Kim, H.; Boudreau, D.; Algar, W.R. Fully self-assembled silica nanoparticle–semiconductor quantum dot supra-nanoparticles and immunoconjugates for enhanced cellular imaging by microscopy and smartphone camera. *ACS Appl. Mater. Interfaces* **2020**, *12*, 33530–33540. [[CrossRef](#)] [[PubMed](#)]
4. Ramazani, A.; Asiabi, P.A.; Aghahosseini, H.; Gouranlou, F. Review on the synthesis and functionalization of  $\text{SiO}_2$  nanoparticles as solid supported catalysts. *Curr. Org. Chem.* **2017**, *21*, 908–922. [[CrossRef](#)]
5. El-Desoky, H.; Abdel-Galeila, M.; Khalifa, A. Mesoporous  $\text{SiO}_2$  (SBA-15) modified graphite electrode as highly sensitive sensor for ultra trace level determination of Dapoxetine hydrochloride drug in human plasma. *J. Electroanal. Chem.* **2019**, *846*, 113157. [[CrossRef](#)]
6. Ismail, S.; Yusof, N.A.; Abdullah, J.; Abd Rahman, S.F. Electrochemical detection of arsenite using a silica nanoparticles-modified screen-printed carbon electrode. *Materials* **2020**, *13*, 3168. [[CrossRef](#)]
7. Bukkittar, S.D.; Shetti, N.P.; Kulkarni, R.M.; Churmure, S. Nano-silica modified electrode as a sensor for the determination of mefenamic acid—A voltammetric sensor. *Mater. Today Proc.* **2018**, *5*, 21466–21473. [[CrossRef](#)]
8. Mathelié-Guinlet, M.; Cohen-Bouhacina, T.; Gammoudi, I.; Martin, A.; Beven, L.; Delville, M.-H.; Grauby-Heywang, C. Silica nanoparticles-assisted electrochemical biosensor for the rapid, sensitive and specific detection of *Escherichia coli*. *Sens. Actuators B* **2019**, *292*, 314–320. [[CrossRef](#)]
9. Tashkhourian, J.; Nami-Ana, S.F. A sensitive electrochemical sensor for determination of gallic acid based on  $\text{SiO}_2$  nanoparticle modified carbon paste electrode. *Mater. Sci. Eng. C* **2015**, *52*, 103–110. [[CrossRef](#)]
10. Tashkhourian, J.; Daneshi, M.; Nami-Ana, S.F. Simultaneous determination of tyrosine and tryptophan by mesoporous silica nanoparticles modified carbon paste electrode using H-point standard addition method. *Anal. Chim. Acta* **2016**, *902*, 89–96. [[CrossRef](#)]
11. Swathi, S.; Rani, B.J.; Ravi, G.; Yuvakkumar, R.; Hong, S.I.; Velauthapillai, D.; Saravanakumar, B.; Thambidurai, M.; Dang, C. Designing rational and cheapest  $\text{SeO}_2$  electrocatalyst for long stable water splitting process. *J. Phys. Chem. Solids* **2020**, *145*, 109544. [[CrossRef](#)]

12. Karuppasamy, P.; Karthika, A.; Senthilkumar, S.; Rajapandian, V. An efficient and highly sensitive amperometric quercetin sensor based on a lotus flower like SeO<sub>2</sub> decorated rGO nanocomposite modified glassy carbon electrode. *Electrocatalysis* **2022**, *13*, 269–282. [[CrossRef](#)]
13. Kavieva, L.; Ziyatdinova, G. Sensitive voltammetric quantification of carminic acid in candies using selenium dioxide nanoparticles based electrode. *Food Chem.* **2022**, *386*, 132851. [[CrossRef](#)] [[PubMed](#)]
14. Merinas-Amo, R.; Martínez-Jurado, M.; Jurado-Güeto, S.; Alonso-Moraga, Á.; Merinas-Amo, T. Biological effects of food coloring in in vivo and in vitro model systems. *Foods* **2019**, *8*, 176. [[CrossRef](#)] [[PubMed](#)]
15. König, J. Food colour additives of synthetic origin. In *Colour Additives for Foods and Beverages*; Scotter, M.J., Ed.; Woodhead Publishing: Cambridge, UK, 2015; pp. 35–60.
16. Jang, J.-Y. The past, present, and future of image-enhanced endoscopy. *Clin. Endosc.* **2015**, *48*, 466–475. [[CrossRef](#)]
17. EFSA ANS Panel. Scientific opinion on the re-evaluation of indigo carmine (E 132) as a food additive. *EFSA J.* **2014**, *12*, 3768. [[CrossRef](#)]
18. Carretero-González, J.; Castillo-Martínez, E.; Armand, M. Highly water-soluble three-redox state organic dyes as bifunctional analytes. *Energy Environ. Sci.* **2016**, *9*, 3521–3530. [[CrossRef](#)]
19. Mo, S.; Na, J.; Mo, H.; Chen, L. Voltammetric determination of indigo carmine and amaranth on a silver-based mercury film electrode. *Anal. Lett.* **1992**, *25*, 899–909. [[CrossRef](#)]
20. Álvarez, M.J.B.; Abedul, M.T.F.; García, A.C. Flow amperometric detection of indigo for enzyme-linked immunosorbent assays with use of screen-printed electrodes. *Anal. Chim. Acta* **2002**, *462*, 31–37. [[CrossRef](#)]
21. Beggiano, G.; Casalbore-Miceli, G.; Geri, A.; Pietropaolo, D. Indigo carmine—An electrochemical study. *Ann. Chim.* **1993**, *83*, 355–363.
22. Díaz-González, M.; Fernández-Sánchez, C.; Costa-García, A. Comparative voltammetric behavior of indigo carmine at screen-printed carbon electrodes. *Electroanalysis* **2002**, *14*, 665–970. [[CrossRef](#)]
23. Silva, T.A.; Pereira, G.F.; Fatibello-Filho, O.; Eguiluz, K.I.B.; Salazar-Banda, G.R. Electroanalytical sensing of indigo carmine dye in water samples using a cathodically pretreated boron-doped diamond electrode. *J. Electroanal. Chem.* **2016**, *769*, 28–34. [[CrossRef](#)]
24. Deroco, P.B.; Medeiros, R.A.; Rocha-Filho, R.C.; Fatibello-Filho, O. Selective and simultaneous determination of indigo carmine and allura red in candy samples at the nano-concentration range by flow injection analysis with multiple pulse amperometric detection. *Food Chem.* **2018**, *247*, 66–72. [[CrossRef](#)] [[PubMed](#)]
25. Arvand, M.; Saberi, M.; Ardaki, M.S.; Mohammadi, A. Mediated electrochemical method for the determination of indigo carmine levels in food products. *Talanta* **2017**, *173*, 60–68. [[CrossRef](#)] [[PubMed](#)]
26. Edwin, D.S.; Manjunatha, J.G.; Raril, C.; Girish, T.; Ravishankar, D.K.; Arpitha, H.J. Electrochemical analysis of indigo carmine using polyarginine modified carbon paste electrode. *J. Electrochem. Sci. Eng.* **2021**, *11*, 87–96. [[CrossRef](#)]
27. Manjunatha, J.G.G. A novel poly (glycine) biosensor towards the detection of indigo carmine: A voltammetric study. *J. Food Drug Anal.* **2018**, *26*, 292–299. [[CrossRef](#)]
28. Stefan-van Staden, R.-I.; van Staden, J.F. Dot microsensors based on zinc porphyrins and zinc phthalocyanine for the determination of indigo carmine. *ECS J. Solid State Sci. Technol.* **2020**, *9*, 041015. [[CrossRef](#)]
29. Hareesha, N.; Manjunatha, J.G.; Amrutha, B.M.; Pushpanjali, P.A.; Charithra, M.M.; Subbaiah, N.P. Electrochemical analysis of indigo carmine in food and water samples using a poly(glutamic acid) layered multi-walled carbon nanotube paste electrode. *J. Electron. Mater.* **2021**, *50*, 1230–1238. [[CrossRef](#)]
30. Incebay, H.; Kilic, A. Electrochemical determination of indigo carmine in food and water samples using a novel platform based on chiral amine-bis(phenolate) boron complex. *Dye. Pigment.* **2022**, *197*, 109921. [[CrossRef](#)]
31. Bard, A.J.; Faulkner, L.R. *Electrochemical Methods: Fundamentals and Applications*, 2nd ed.; John Wiley & Sons: New York, NY, USA, 2001; 864p.
32. Gnanam, S.; Rajendran, V. Influence of various surfactants on size, morphology, and optical properties of CeO<sub>2</sub> nanostructures via facile hydrothermal route. *J. Nanopart.* **2013**, *2013*, 839391. [[CrossRef](#)]
33. Ziyatdinova, G.; Ziganshina, E.; Romashkina, S.; Budnikov, H. Highly sensitive amperometric sensor for eugenol quantification based on CeO<sub>2</sub> nanoparticles and surfactants. *Electroanalysis* **2017**, *29*, 1197–1204. [[CrossRef](#)]
34. Karuppiah, S.; Thangaraj, S.; Palaniappan, S.A.; Lakshmanan, S.O. Influence of surfactants on structural, morphological, optical and antibacterial properties of SnO<sub>2</sub> nanoparticles. *IET Nanobiotechnol.* **2019**, *13*, 952–956. [[CrossRef](#)] [[PubMed](#)]
35. Bhattacharjee, A.; Ahmaruzzaman, M.; Sinha, T. Surfactant effects on the synthesis of durable tin-oxide nanoparticles and its exploitation as a recyclable catalyst for the elimination of toxic dye: A green and efficient approach for wastewater treatment. *RSC Adv.* **2014**, *4*, 51418–51429. [[CrossRef](#)]
36. Ziyatdinova, G.; Budnikov, H. Carbon nanomaterials and surfactants as electrode surface modifiers in organic electroanalysis. In *Nanoanalytics: Nanoobjects and Nanotechnologies in Analytical Chemistry*; Shtykov, S.N., Ed.; De Gruyter: Berlin, Germany; Boston, MA, USA, 2018; pp. 223–251.
37. Ziyatdinova, G.; Yakupova, E.; Davletshin, R. Voltammetric determination of hesperidin on the electrode modified with SnO<sub>2</sub> nanoparticles and surfactants. *Electroanalysis* **2021**, *33*, 2417–2427. [[CrossRef](#)]
38. Ziyatdinova, G.K.; Zakharova, S.P.; Ziganshina, E.R.; Budnikov, H.C. Voltammetric determination of flavonoids in medicinal plant materials using electrodes modified by cerium dioxide nanoparticles and surfactants. *J. Anal. Chem.* **2019**, *74*, 816–824. [[CrossRef](#)]

39. Ziyatdinova, G.; Ziganshina, E.; Shamsevalieva, A.; Budnikov, H. Voltammetric determination of capsaicin using CeO<sub>2</sub>-surfactant/SWNT-modified electrode. *Arab. J. Chem.* **2020**, *13*, 1624–1632. [[CrossRef](#)]
40. Wang, W.; Gu, B.; Liang, L. Effect of surfactants on the formation, morphology, and surface property of synthesized SiO<sub>2</sub> nanoparticles. *J. Dispers. Sci. Technol.* **2005**, *25*, 593–601. [[CrossRef](#)]
41. Lasia, A. *Electrochemical Impedance Spectroscopy and Its Applications*; Springer: New York, NY, USA, 2014; 367p.